Relationship between the Crystal Structure and Morphology of Carboxylic Acid Polymorphs. Predicted and Experimental Morphologies

ARTICLE *in* CRYSTAL GROWTH & DESIGN · SEPTEMBER 2010

Impact Factor: 4.89 · DOI: 10.1021/cg901436p

4 AUTHORS:

Evelyn Moreno-Calvo
Spanish National Research Council
31 PUBLICATIONS **238** CITATIONS
SEE PROFILE

Teresa Calvet
University of Barcelona
203 PUBLICATIONS **1,615** CITATIONS
SEE PROFILE

Miguel Angel Cuevas-Diarte
University of Barcelona
168 PUBLICATIONS **1,078** CITATIONS
SEE PROFILE

Dino Aquilano
Università degli Studi di Torino
190 PUBLICATIONS **999** CITATIONS
SEE PROFILE

DOI: 10.1021/cg901436p

CRYSTAL GROWTH & DESIGN Article

2010, Vol. 10
4262–4271

Relationship between the Crystal Structure and Morphology of Carboxylic Acid Polymorphs. Predicted and Experimental Morphologies

Evelyn Moreno-Calvo,*,† Teresa Calvet,† Miguel Angel Cuevas-Diarte,*,† and Dino Aquilano‡

†*Departament de Cristal·lografia, Mineralogia i Dipòsits Minerals, Facultat de Geologia, Universitat de Barcelona, C/Martí i Franquès s/n, 08028 Barcelona, Spain, and* ‡*Dipartimento di Scienze Mineralogiche e Petrologiche, Università degli Studi di Torino, via V. Caluso 35, 10125 Torino, Italy*

Received November 17, 2009; Revised Manuscript Received July 30, 2010

ABSTRACT: Polymorphs of carboxylic acids crystallize from solvent evaporation experiments as crystals with needle or plate morphology. Experimentally, it has been observed that the crystallization solvent does not sensibly modify the crystal morphology of a given polymorph. Hence, a theoretical study of the morphology of these polymorphs was conducted to relate the crystal structures with their macroscopic crystal shapes. Methodologies with an increasing degree of complexity were used, and the best results were obtained from those calculations considering the attachment energy (E_{att}^{hkl}) released on attachment of a new d_{hkl} layer to a growing crystal surface. The experimental habits of the polymorphs of carboxylic acids are reproduced well by the morphology simulations, so the observed crystal shapes can be rationalized in terms of the intermolecular interactions between the growth units. In the crystal structures of the C, B, and E polymorphs, layers of pure CH_3 residues produce weak van der Waals interactions resulting in strongly anisotropic crystal growth (platy crystals) with highly developed {100} faces.

Introduction

Crystal morphology is a key element in many industrial processes and has an enormous impact at the processing and postprocessing stages of pharmaceuticals, agrochemicals, petrochemicals, and cements. The morphology of crystalline solids influences their physical properties. Crystal morphology can alter the dissolution rate of chemicals and bioavailability of drugs and mechanical properties such as filtration, grinding, dusting and handling, and packaging and storage of crystalline products.

Prediction of crystal morphology can also be used as a tool for the rational design of experimental work. For example, Tedesco[1] and co-workers improved the industrial processing of a drug for the treatment of asthma by modifying its morphology. Predicted crystal morphology allowed researchers to study the chemical entities emerging from different cleaved crystal surfaces and modify the crystal habit on the basis of different interactions with solvent. They concluded and experimentally demonstrated that working with polar solvents would diminish the crystal size while nonpolar solvents would produce elongated crystals. S. L. Price[2] used morphology predictions to reduce the number of probable polymorphs of paracetamol because those with low calculated growth rates and plate morphologies were unlikely to form in comparison to the rest. In the biomedical field, a rational pathway for antimalaria drug design was proposed on the basis of crystal morphology.[3] Researchers at the Weizmann Institute of Science (Rehovot, Israel) and Transform Pharmaceuticals (Lexington, MA) used crystal morphology to study quinoline-binding sites on malaria−pigment crystals, the byproduct of digestion of hemoglobin by the malaria parasite. They modeled the formation of malaria−pigment crystals and used this information to propose binding sites for quinoline-based antimalarial drugs.[3]

Thus, rationalization of the relationships between crystal morphology and the arrangement of atoms in the bulk crystal lattice is of great interest in many areas of science.[4,5]

In this work, we study the crystal morphologies of seven polymorphs of even *n*-saturated carboxylic acids ranging from $C_{10}H_{19}O_2H$ to $C_{20}H_{39}O_2H$. There has been much work dealing with the crystal structure analysis, polymorphic occurrence, and crystal shape observation of the different polymorphs of carboxylic acids.[6−9] In these studies, the crystal shape proved to be a key characteristic in the identification of the different polymorphs. In light of the previous findings, we wanted to provide a comprehensive understanding of the crystal structure−morphology relationships of a series of polymorphs of even saturated carboxylic acids and to complete similar studies of *n*-alkanes[10] and *n*-dicarboxylic acids.[11] In addition, carboxylic acids make up one of the basic families of organic crystals widely distributed in nature (oils, lipid membranes, and cosmetics), and an understanding of them is necessary to expand to more complex systems such as fats and oils.[12]

Experimental Section

Chemicals. Acids $C_{10}H_{19}O_2H$, $C_{12}H_{23}O_2H$, $C_{14}H_{27}O_2H$, and $C_{16}H_{31}O_2H$ were purchased from Fluka and acids $C_{18}H_{35}O_2H$ and $C_{20}H_{39}O_2H$ from Aldrich.

Crystallization Experiments. Solvents used in the crystallization experiments were chosen so they covered a broad range of polarity and functional groups. The following solvents were used without further purification: *n*-pentane, isooctane, toluene, chloroform, diethyl ether, and ethanol. Two types of methods were used to obtain polycrystalline powder samples. (1) Slow evaporations of the solvent were performed by allowing the solvent to evaporate in pierced crystallization vessels at 298 K, and (2) rapid evaporations were performed at room temperature by passing a nitrogen gas stream over a saturated solution.

*To whom correspondence should be addressed. E-mail: evemoreno@ub.edu or macuevasdiarte@ub.edu. Telephone: +34-93-402.13.50. Fax: +34-93-402.13.40.

Published on Web 09/10/2010

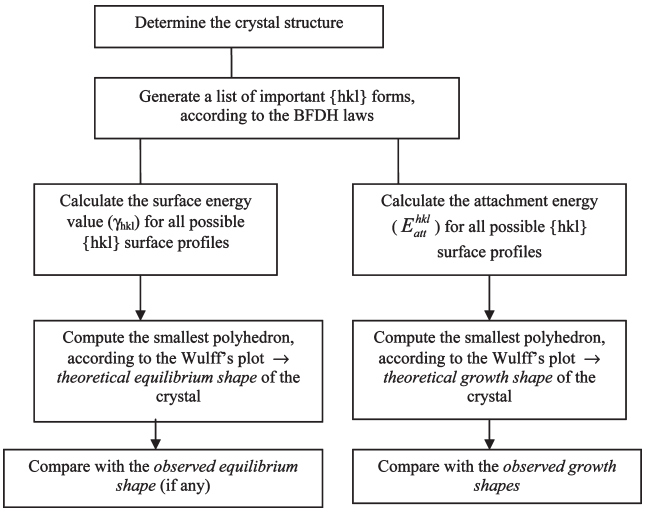

Figure 1. Flowchart to be followed to predict both equilibrium (EQM) and growth morphology evaluated through the attachment energy (AE) of a crystal.

Optical Micrographs (OM). Optical micrographs of all the samples were taken using a Nikon Eclipse LV100 POL microscope to study the overall macroscopic crystal habit of the different polymorphs.

Predicting Growth and Equilibrium Morphology. Three methods are commonly used to predict the morphology from the knowledge of the crystal structure. A workflow is given in Figure 1.

The Bravais−Friedel Donnay−Harker (BFDH) laws[13−15] are strictly based on the symmetry of the crystal lattice to generate an ordered list of possible growing faces. The relative growth rate of $\{hkl\}$ forms (R_{hkl}) is inversely proportional to the interplanar distance d_{hkl} (eq 1). The larger the d_{hkl}, the more pronounced the morphological importance (MI) of the face, implicitly reflecting the weakest interactions between the content of adjacent d_{hkl} layers.

$$R_{hkl} \propto 1/d_{hkl} \tag{1}$$

The method based on the attachment energy (AE), proposed by Hartman and Perdok[16] and Hartman and Bennema,[17] are based on the interactions occurring between the growth units during the crystallization process. In Hartman−Perdok theory, the crystal faces $\{hkl\}$ are classified into three categories depending on the number of PBCs running within a d_{hkl} slice. A PBC is an uninterrupted, stoichiometric, and periodic chain made of bonds (in the first coordination sphere) between consecutive growth units.

A d_{hkl} slice, obeying the systematic extinction rules and containing at least two families of parallel PBCs, determines a flat (F) face, while a slice containing only one kind of parallel PBCs determines a stepped (S) face. Finally, those faces that are not parallel to any PBC are the so-called kinked (K) faces.

If one considers a slide of thickness $d_{hkl}/2$ (such as the slice of thickness d_{002} in the NaCl crystal), the stoichiometric content of the crystal can be found at the intersection of two PBCs. This represents an equilibrium site of the crystal (the so-called "kink" position) and allows evaluation of the crystallization energy (E_{cr}) released when a "formula unit", coming from the mother phase, enters the crystal (Figure 2).

The crystallization energy is a constant for a given crystal and hence does not vary from face to face. Using Figure 2, E_{cr} may be decomposed into two parts: E_{slice}^{hkl}, i.e., the energy released when the crystallizing formula unit laterally binds to the content of half the slice, and E_{att}^{hkl}, i.e., the energy released when the crystallizing formula unit vertically binds to the underlying crystal. This can be expressed by the fundamental relationship

$$E_{cr} = E_{slice}^{hkl} + E_{att}^{hkl} = \text{constant} \tag{2a}$$

Hartman and Perdok[16] assumed and demonstrated that R_{hkl}, the normal growth rate of a (hkl) face, is proportional to its attachment energy:

$$R_{hkl} \propto E_{att}^{hkl} \tag{2b}$$

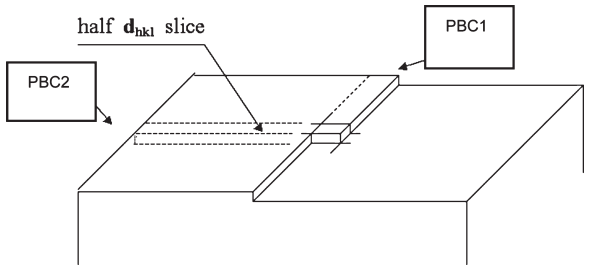

Figure 2. Scheme of the crystallization mechanism by the addition of a crystallization unit at the intersection of two PBCs.

It ensues that the higher the slice energy of a given face, the lower its attachment energy and hence its normal growth rate; consequently, the growth shape of a crystal will be dominated by those $\{hkl\}$ forms showing the lowest E_{att}^{hkl} values. Flat faces, as shown in Figure 2, develop strong interactions within their slices, while S and K faces do not exhibit important (if any) correlations between adjacent chains in the slice; therefore, their growth rate will be higher than that of the F faces, and they usually tend to disappear from the growth morphology.

The Hartman−Perdok method, thanks to the constraints due to the electrical stability of the d_{hkl} slices, allows us to find all the possible profiles of a given face, as it follows from the choice of all possible kinds of PBCs running along a given $[uvw]$ direction. Once the $\{hkl\}$ profiles are obtained, the corresponding surface energy values γ_{hkl} can be calculated, to determine the equilibrium morphology (EQM) of the crystal, i.e., the shape that minimizes, at a constant volume,[18,19] the total surface energy of a crystal.

Surface energy, for unrelaxed surface structures, is simply defined within the Born−Stern approximation:

$$\gamma_{hkl} = \frac{W_{hkl}^{sep}}{2A_{hkl}} \tag{3a}$$

where W_{hkl}^{sep} represents the work to be spent to separate into two parts a crystal along the hkl plane, thereby creating two equivalent surfaces of area A_{hkl}. A practical way to calculate the γ_{hkl} values is to use an infinite $M \times d_{hkl}$ slab and compare the difference between the energy of the slice within the crystal bulk,[20] $E_{bulk}(M)$, and the energy of the same slice exposed to the vacuum, $E_{slice}(M)$:

$$\gamma_{hkl} = \lim_{M \to \infty} \frac{[E_{bulk}(M) - E_{slice}(M)]}{2A_{hkl}} \tag{3b}$$

Two considerations are to be taken into account: The values so obtained refer to a temperature of 0 K (entropic contributions are not considered), and their variations due to the adsorption of a condensed mother phase (solution, melt) are neglected as well.

Determining the equilibrium shape of a crystal is extremely important because the weighted average of the γ_{hkl} values represents the rate-determining factor, at a constant temperature, of the three-dimensional nucleation frequency of crystals. Further, knowing all the allowed γ_{hkl} values for a given $\{hkl\}$ form is fundamentally important for finding the most probable hkl surface profile, on which a foreign phase (melt, solvent, and impurities) could occur.

Computer Morphology Simulation. Morphology predictions were performed using the Morphology and Forcite tools implemented in Materials Studio[20] version 4.2. Crystal structures used to simulate morphology were determined from powder X-ray diffraction data,[8,9] unless specified in the text. Their crystallographic information files (CIF) are deposited within the CCDC.

In each case, a list of growth faces is generated according to the Donnay−Harker rules. The minimum interplanar spacing for face list generation was set to 1.3 Å, and the maximum absolute values for the Miller indices h, k, and l for the faces were set to 3, 3, and 3, respectively, with an upper limit of 200 growing faces. After face generation, the chosen algorithm (BFDH, AE, or EQM) is applied and the attachment or surface energy is calculated accordingly using the COMPASS2[21] force field.

Scheme 1. Schematic molecular arrangements shown in the solid state by the polymorphs B_o, B_m, E_o, E_m, C, A_{super} and A_1 of carboxylic acids ($0 \leq n \leq 10$). The crystal structures of the A_2 and A_3 polymorphs are still unknown

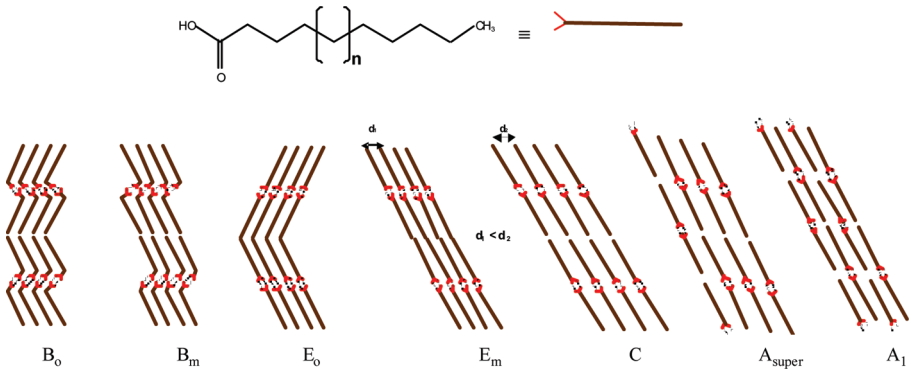

Table 1. Crystallographic Data for the Polymorphs of the Different Carboxylic Acids Used To Simulate the Crystal Morphology

	a (Å)	*b* (Å)	*c* (Å)	α (deg)	*β* (deg)	*γ* (deg)	source
			Polymorph C, $P2_1/c$ $Z = 4$				
$C_{10}H_{19}O_2H$	23.10(1)	4.940(1)	9.834(1)	90	90.01(1)	90	powder
$C_{12}H_{23}O_2H$	27.54(1)	4.953(1)	9.604(1)	90	97.28(1)	90	powder
$C_{14}H_{27}O_2H$	31.63(1)	4.967(1)	9.492(1)	90	95.10(1)	90	powder
$C_{16}H_{31}O_2H$	35.72(1)	4.975(1)	9.439(1)	90	90.39(1)	90	powder
$C_{18}H_{35}O_2H$	39.99(1)	4.960(1)	9.354(1)	90	95.00(1)	90	powder
$C_{20}H_{39}O_2H$	44.12(1)	4.965(1)	9.318(1)	90	93.69(1)	90	powder
			Polymorph B_m, $P2_1/c$ $Z = 4$				
$C_{16}H_{31}O_2H$	39.44(1)	7.410(1)	5.589(1)	90	92.96(1)	90	powder
$C_{18}H_{35}O_2H$	43.95(2)	7.397(1)	5.598(1)	90	90.31(1)	90	powder
$C_{20}H_{39}O_2H$	48.43(1)	7.404(1)	5.582(1)	90	93.11(1)	90	powder
			Polymorph E_m, $P2_1/c$ $Z = 4$				
$C_{16}H_{31}O_2H$	39.72(1)	7.374(1)	5.614(1)	90	90.13(1)	90	powder
$C_{18}H_{35}O_2H$	44.26(1)	7.386(1)	5.608(1)	90	93.25(1)	90	powder
$C_{20}H_{39}O_2H$	48.76(1)	7.377(1)	5.603(1)	90	90.88(1)	90	powder
			Polymorph B_o, *Pbca* $Z = 8$				
$C_{18}H_{35}O_2H$	7.408(3)	5.587(3)	87.69(6)	90	90	90	powder
$C_{20}H_{39}O_2H$	7.414(1)	5.592(1)	96.74(1)	90	90	90	powder
			Polymorph E_o, *Pbca* $Z = 8$				
$C_{18}H_{35}O_2H$	7.359(3)	5.609(1)	88.41(5)	90	90	90	single crystal
			Polymorph A_{super}, $P\bar{1}$ $Z = 6$				
$C_{12}H_{23}O_2H$	5.415(1)	17.900(4)	21.370(4)	111.10(3)	97.03(2)	90.63(4)	single crystal
			Polymorph A_1, $P\bar{1}$ $Z = 2$				
$C_{12}H_{23}O_2H$	5.400(2)	7.450(3)	15.989(5)	88.57(4)	86.73(3)	98.30(1)	single crystal

Results and Discussion

Crystal Structures and Polymorphism of Carboxylic Acids. Carboxylic acids are extremely rich in polymorphic forms.[6] Each of the even members of the carboxylic acids' family with a carbon content between 10 and 20 can crystallize into nine different polymorphs (A_1, A_2, A_3, A_{super}, E_o, E_m, B_o, B_m, and C). All polymorphs transform to the C form before melting via a first-order solid−solid transition. Consequently, the A-, E-, and B-type polymorphs are called the low-temperature polymorphs and the C-type polymorphs the high-temperature polymorphs.

In general terms, the packing of even carboxylic acid polymorphs consists of bilayers formed by dimers united through a typical $R_2^2(8)$ hydrogen bond pattern according to graph set notation.[22] The plane between bilayers is composed of pure methyl or pure carboxyl groups for the cases of the C-, B-, and E-type polymorphs. In the case of the A-type polymorphs, methyl and carboxylic groups coexist in the same interlayer interface. In the A_{super} structures, the unit cell is composed of six molecules arranged in such a way that within a monolayer three adjacent molecules have their carboxyl groups pointing in one direction and the next three molecules have the carboxyl group pointing in the opposite direction. However, for A_1, the structure is such that, within a monolayer, the carboxyl group of one molecule is adjacent to the methyl group of the neighboring molecule. Molecules of the different polymorphs have an *all-trans* conformation, except molecules of the A-type polymorphs that show a distortion involving the C_1-C_2 bond and molecules of the B-type polymorphs that adopt the *gauche* conformation around the C_2-C_3 bond.

The crystal packing of the different polymorphs is shown in Scheme 1.

In previous studies, the crystal structures of seven different polymorphs have been determined for some members of the family using single-crystal or powder X-ray diffraction sources.[7−9] Relevant crystallographic data of the carboxylic acids' polymorphs used in this study are listed in Table 1.

Crystallization Experiments. Systematic crystallization experiments were performed using the techniques and solvents

Table 2. Summary of Crystallization Experiments[a]

	rapid evaporation			slow evaporation		
	WPS[b]	IPS[c]	SPS[d]	WPS[b]	IPS[c]	SPS[d]
$C_{14}H_{27}O_2H$	A_2 [dendrite]	A_2 [dendrite]	C (A_2) [rhombus 54° (dendrite)]		A_{super} (C) [nedlee (rhombus 54°)]	C [rhombus 54°]
	A_{super} [nedlee]	A_{super} [nedlee]		C [rhombus 54°]		
	C [rhombus 54°]	C [rhombus 54°]		A_2 [dendrite]		
$C_{16}H_{31}O_2H$	A_2 [dendrite]		C [rhombus 54°]		C [rhombus 54°]	B_m [rhombus 74°]
	C [rhombus 54°]	E_m (E_o) [rhombus 74°]		C [rhombus 54°]	A_{super} [nedlee]	
	E_m (E_o) [rhombus 74°]	C [rhombus 54°]		A_2 [dendrite]	B_m [rhombus 74°]	
$C_{18}H_{35}O_2H$	E_m [rhombus 74°]	E_m (E_o) [rhombus 74°]	–	B_o [rhombus 74°]	B_o [rhombus 74°]	–
	C [rhombus 54°]			B_m [rhombus 74°]	B_m [rhombus 74°]	
				A_2 [dendrite]	A_2 [dendrite] E_m [rhombus 74°] C [rhombus 54°]	
$C_{20}H_{39}O_2H$	E_m [rhombus 74°]	E_m (E_o) [rhombus 74°]	–	B_o [rhombus 74°]	B_o [rhombus 74°] E_m [rhombus 74°] B_m (B_o) [rhombus 74° (rhombus 74°)]	–

[a] The polymorph obtained from each experiment is listed followed by their crystal shape in brackets. Acute angles of 54° or 74° are formed at the intersection of the rhombus sides. If a mixture of polymorphs was obtained, the polymorph obtained in the minor proportion is listed in parentheses. [b] WPS refers to weak polar solvents (pentane and isooctane). [c] IPS refers to intermediate polar solvents (toluene, chloroform, and ether). [d] SPS refers to strong polar solvents (ethanol).

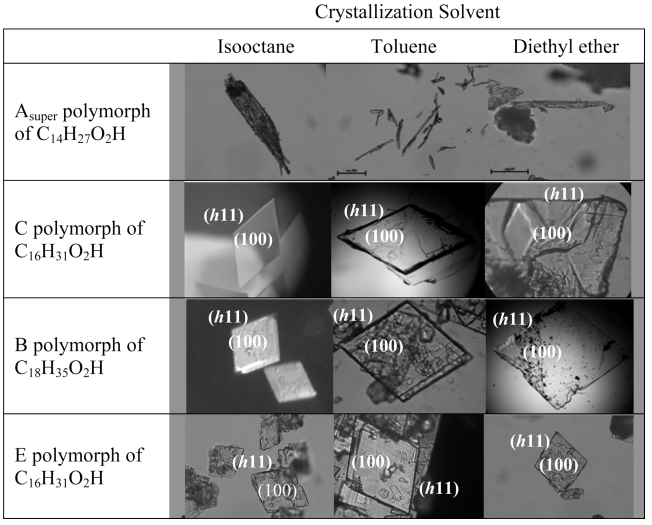

Figure 3. Images of the growth morphologies of four carboxylic acid polymorphs grown from isooctane, toluene, and diethyl ether taken with the optical microscope. The nature of the polymorph obtained was determined by powder X-ray diffraction. The faces are labeled according to their orientation and the BFDH laws. Indices *h* are not specified as they are difficult to determine experimentally.

described in the Experimental Section. A summary of the results obtained is given in Table 2. The polymorphic nature of the solids obtained in each crystallization experiment was checked by powder X-ray diffraction and is listed in Table 2 followed by the observed morphology of the crystallites.

Experimental Morphologies. Representative photographic images of the growth morphologies of carboxylic acids obtained from the crystallizations listed in Table 2 are presented and indexed in Figure 3. In light of the observed morphologies, we can conclude that (i) crystals of the E- and B-type polymorphs crystallize as rhombus-shaped crystals with an acute angle of 74°, (ii) crystals of the C polymorph also form rhombus-shaped crystals, but with an acute angle of 54°, and (iii) crystals of the triclinic polymorph A_{super} crystallize with a needlelike shape. These characteristic morphologies have been observed to be independent of the (i) polarity, (ii) nature of the solvent, and (iii) rate of crystallization. Therefore, it seems that the morphology of a given polymorph is not significantly influenced by the crystallization solvent. This result disagrees with the behavior of other long chain compounds such as dicarboxylic acids in which the crystal morphology is highly dependent on the crystallization solvent.[11,23] The independence of the morphology from the crystallization solvent is explained in the following sections on the basis of the crystal structures of each polymorph.

The monoclinic C-, E-, and B-type polymorphs of carboxylic acids (all belonging to space group $P2_1/c$) give very thin crystals showing well-developed {100} top faces and poorly developed side faces. This type of growth occurs because the energy release upon attachment of a new crystallizing unit to both the {100} faces, terminated by methyl groups (weak van der Waals interactions), is smaller than that for addition of a new growing unit laterally (where strong hydrogen bonds and van der Waals interactions develop). The weakest interactions are almost perpendicular to the (100) plane, while the strongest interactions are within the main plane of the molecular dimer arrangement. Consequently, the top {100} faces grow slowly and dominate the morphology while side faces growth relatively fast, either disappearing from the morphology or appearing as thin faces. Especially for anisotropic crystal structures such as carboxylic acids, there are large differences in the interactions in different directions along the various faces.

Comparison of the BFDH, Attachment Energy, and Equilibrium Morphology Methods. Figure 4 shows the morphology of acid $C_{16}H_{31}O_2H$ in the C polymorph ($P2_1/c$, $Z = 4$) predicted using the BFDH laws, the AE method, and the EQM method.

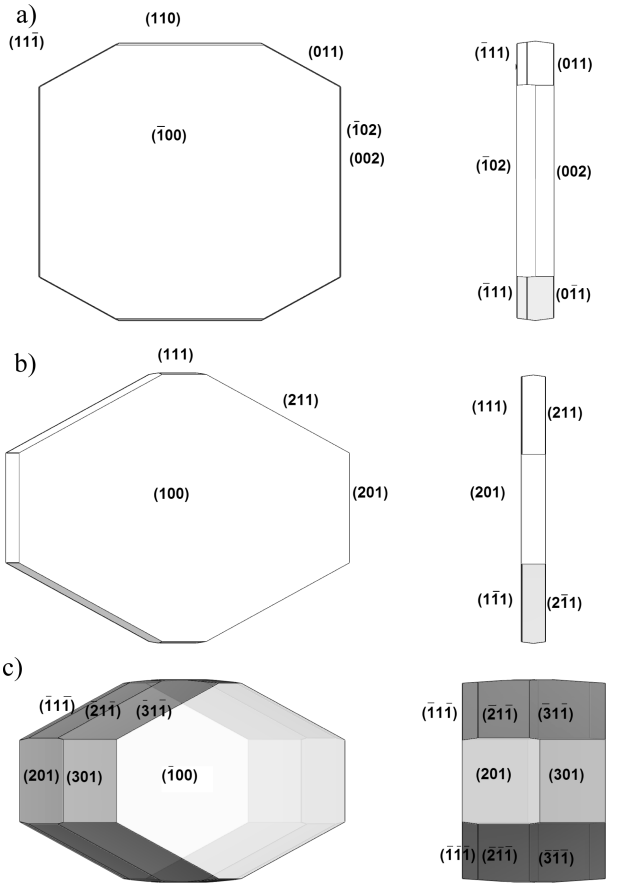

Figure 4. Predicted morphology of the C polymorph of $C_{16}H_{31}O_2H$. (a) Growth shape from BFDH rules. (b) Growth shape from attachment energy calculation. (c) Equilibrium shape. For each prediction method, two pictures are drawn, one viewed from the top and one from the side. The *b* axis is chosen as the common vertical axis (north−south direction) in all drawings.

Table 3. Predicted Forms of Acid $C_{16}H_{31}O_2H$ in the C Polymorph ($P2_1/c$, $Z = 4$) Using the BFDH Laws Followed by Their Multiplicity and Interplanar Spacing

{*hkl*}	multiplicity	d_{hkl} (Å)
{100}	2	35.64
{110}	4	4.78
{10$\bar{2}$}	2	4.37
{001}	2	4.37
{011}	4	4.22
{11$\bar{1}$}	4	4.21

The forms that are most morphologically important, predicted using the BFDH laws, are listed in Table 3. The value of d_{hkl} can be calculated from the elementary cell dimensions in Table 1.

The differences between the predicted growth shapes (BFDH and attachment energy methods) and the predicted equilibrium shape are quantified in Table 4 for acids $C_{10}H_{19}O_2H$ and $C_{20}H_{39}O_2H$ in the C form. These results are representative of the six acids investigated. Morphologies were evaluated assuming, for the growth forms, that the growth rate of a face is proportional either to the magnitude of its interplanar distance (BFDH) or to the attachment energy (AE). With regard to the equilibrium shape, the distance of a {*hkl*} form from the center of the equilibrium polyhedron is proportional to its surface energy value, according to the Gibbs−Wulff theorem. Further, the first and second forms are tabulated for each crystal structure along with its relative total area.

The systematic simulation of the C polymorphs of carboxylic acids has shown that the AE method reproduces the experimental crystal shape with good accuracy. The C polymorph crystallizes from solvents into rhombus-shaped crystals with an acute angle of ~54°, irrespective of the acid chain length or nature of the solvent (Figure 3). In these crystals, the {100} faces are the most developed and, consequently, have the lowest attachment energy as computed using the AE method. Using the BFDH rules, a platelike morphology is predicted as well (Figure 4a). In this case, beyond the {100} faces that are predicted as the most developed ones, new additional small faces that do not appear in the observed habit are also predicted. This occurs because the directionality of the main intermolecular interactions (hydrogen bonds) responsible for this particular crystal growth is not considered.

The experimental morphologies do not show developed side faces. This is not surprising because the same feature is currently observed in both alcohols[24] and normal alkanes,[10] which show the same crystal packing of our carboxylic acids. In fact, the growth kinetics of the basal faces of these compounds is ruled mainly by the spiral mechanism[10g,h] (slow growth), while the surface structure of the lateral faces favors the two-dimensional nucleation mechanism (fast growth): then, the resultant crystal habit must be very flat (the basal faces are those that are crossed by the development axis of the molecular chain). The BFDH method takes into account energetic factors only indirectly, because, for a given d_{hkl} value, the variety of the corresponding surface profiles is not considered in the evaluation of the morphological importance of a given {*hkl*} form; hence, a given number of well-developed

Table 4. Morphology Predictions for the C Polymorph ($P2_1/c$, $Z = 4$) of $C_{10}H_{19}O_2H$ and $C_{20}H_{39}O_2H$

	growth morphology (BFDH)			growth morphology (AE)			equilibrium morphology		
	predicted forms[a]	total area[b] (%)	d_{hkl} (Å)	predicted forms[a]	total area[b] (%)	E_{att} (kJ/mol)	predicted forms[a]	total area[b] (%)	$E_{surface}$ ($\times 10^{25}$ erg cm^{-2} mol^{-1})
$C_{10}H_{19}O_2H$	{100} (2)	71.5	23.09	{100} (2)	77.8	−8.8	{100} (2)	36.9	4
	{001} (2)	5.8	4.42	{111} (4)	16.6	−59.4	{111} (4)	20.7	5
$C_{20}H_{39}O_2H$	{100} (2)	83.2	43.92	{100} (2)	87.1	−8.8	{100} (2)	39.8	4
	{001} (2)	5.9	4.36	{311} (4)	8.36	−113.9	{311} (4)	37.3	5

[a] The two most morphologically important forms, the slowest growing forms, predicted by each method are given followed by their multiplicity (in parentheses). [b] Total area calculated as 100 × [(total surface area of the form)/(total surface area)].

Table 5. Prediction of the Growth Morphology of the C Polymorphs ($P2_1/c$, $Z = 4$) of Acids from $C_{10}H_{19}O_2H$ to $C_{20}H_{39}O_2H$ Using the Method Based on the Attachment Energy (AE)

	predicted forms[a] (multiplicity)	E_{att} (kJ/mol)	total area of the form[b] (%)
$C_{10}H_{19}O_2H$	{100} (2)	−8.8	77.8
	{111} (4)	−59.4	16.6
	{110} (4)	−69.2	0.1
	{101} (2)	−69.8	5.6
$C_{12}H_{23}O_2H$	{100} (2)	−8.8	80.6
	{111} (4)	−70.4	13.9
	{110} (4)	−79.7	0.6
	{101} (2)	−82.6	4.8
$C_{14}H_{27}O_2H$	{100} (2)	−8.8	82.8
	{211} (4)	−81.3	11.9
	{110} (4)	−90.0	1.0
	{201} (2)	−95.2	4.2
$C_{16}H_{31}O_2H$	{100} (2)	−8.8	84.5
	{211} (4)	−92.1	10.4
	{110} (4)	−100.4	1.2
	{201} (2)	−107.9	3.8
$C_{18}H_{35}O_2H$	{100} (2)	−8.8	85.9
	{211} (4)	−103.0	9.3
	{110} (4)	−110.8	1.3
	{201} (2)	−120.5	3.5
$C_{20}H_{39}O_2H$	{100} (2)	−8.8	87.1
	{311} (4)	−113.9	8.3
	{110} (4)	−121.1	1.4
	{301} (2)	−133.1	3.2

[a] The forms present in the predicted morphologies are given followed by their multiplicity (in parentheses). The attachment energy of each form and their corresponding total area are also given. [b] Total area calculated as 100 × [(total surface area of the form)/(total surface area)].

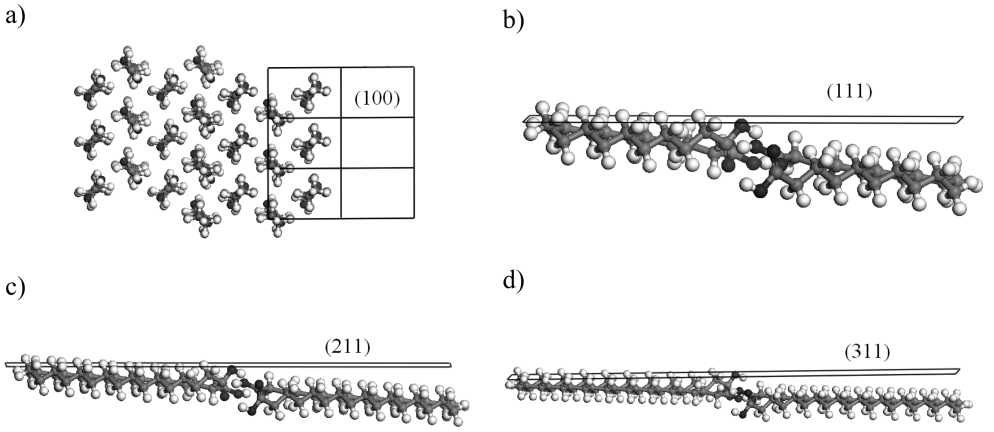

Figure 5. (a) Representation of the (100) face of $C_{20}H_{39}O_2H$, in the C polymorph, showing the terminal methyl groups that gather in the (100) face. (b−d) Representations of the (h11) face of $C_{10}H_{19}O_2H$, $C_{16}H_{31}O_2H$, and $C_{20}H_{39}O_2H$, respectively, in the C polymorph, showing the lateral offset of the chains with respect to the (h11) face.

side faces such as the {110} face are predicted, at variance with the observation.

On the other hand, predictions based on the attachment energy reproduce better the high ratio between the growth rate of the lateral faces (like {110} and {h11}) and that of the basal ones. In fact, the attachment energy can be viewed as the probability of adhesion of a molecule coming from the mother phase and sticking on a given crystal surface. In the case of the carboxylic acids, this probability is very high for a molecule impinging a lateral face, because of the formation of strong bonds between lateral chains, while the probability strongly decreases for molecules going to a crystal site on the basal faces because of the weak interaction between the terminal groups of facing chains.

Thus, it is not surprising that the predictions based on the attachment energy reproduce the observed morphologies better than the BFDH method.

With regard to the predicted equilibrium morphology of the crystals of the C polymorph, the discrepancy between the theoretical equilibrium shape and the experimental (or theoretical) growth shape is more important than one could expect (see Figure 4c), because the calculated equilibrium shape is much more isotropic than the growth shapes (both theoretical and experimental). On one side, this is a general effect that is common to both inorganic and organic crystals. On the other hand, it should be mentioned that the plain difference between the equilibrium and growth shape in carboxylic acids can be attributed to the importance of the second neighbors that heavily intervene in the calculation of the surface energy, while they do play a role to a lesser extent when the attachment energy is evaluated.

Morphology Simulation of the High-Temperature (C-type) Polymorphs of Carboxylic Acids. Table 5 quantifies the predicted morphologies of the C polymorphs of acids $C_{10}H_{19}O_2H$, $C_{12}H_{23}O_2H$, $C_{14}H_{27}O_2H$, $C_{16}H_{31}O_2H$, $C_{18}H_{35}O_2H$, and $C_{20}H_{39}O_2H$ using the method based on the attachment energy. In all cases, the predicted habit is that of an eight-edge flat

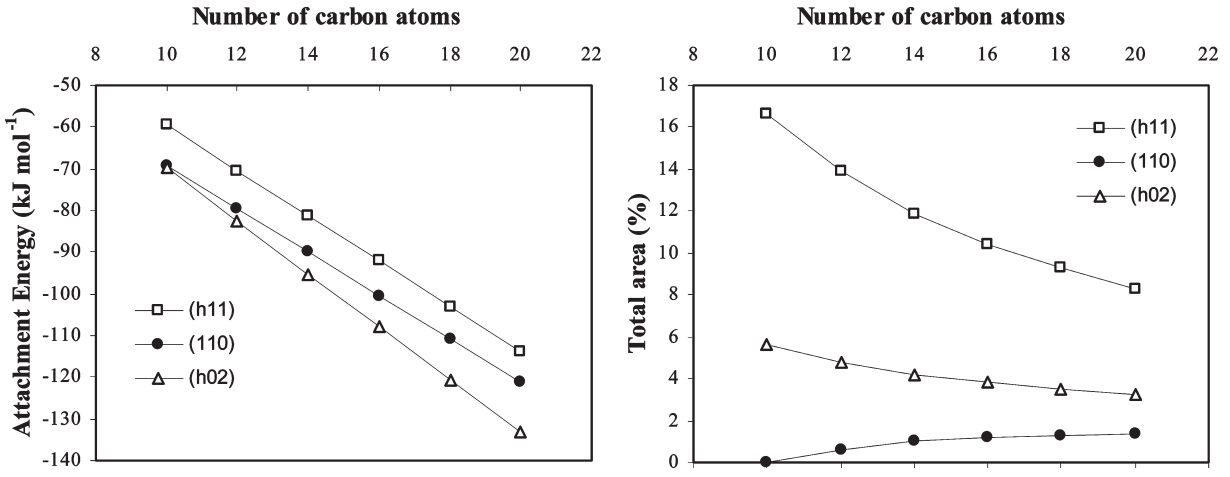

Figure 6. Variation of the attachment energy and the associated total area of (h11), (110), and (h02) faces as a function of the carbon content in the acid chain. The attachment energy variation can be fitted to the equations $E_{att}\{h11\} = -5.4n - 5.0$ ($R^2 = 1$), $E_{att}\{110\} = -5.2n - 17.4$ ($R^2 = 1$), and $E_{att}\{h02\} = -6.3n - 6.7$ ($R^2 = 1$).

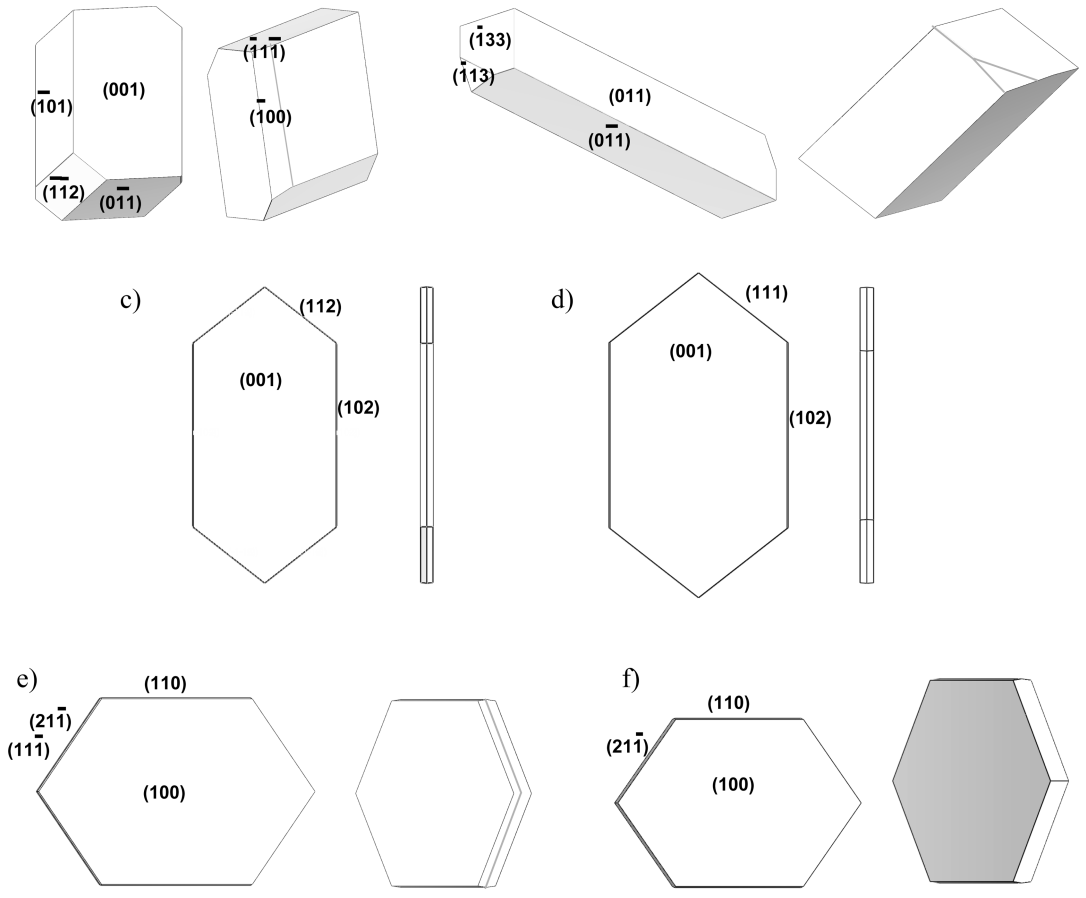

Figure 7. Morphology of (a) A_1 and (b) A_{super} polymorphs of $C_{12}H_{23}O_2H$ and (c) E_o, (d) B_o, (e) E_m, and (f) B_m polymorphs of $C_{18}H_{35}O_2H$ based on the attachment energy (AE) prediction. For each polymorph, two crystals are drawn, the first projected on the (b,a) plane and the second on the (b,c) plane.

plate (Figure 4b) that fairly agrees with the experimental crystal shape.

The results show the presence of a very developed {100} form that represents more than 77% of the total area. The attachment energy associated with the (100) face is −8.8 kJ/mol per molecule and is independent of acid chain length. This fact can be explained in view of Figure 5a. The interactions at the bilayer interface in the crystal structures of the C forms are methyl−methyl interactions. These interactions do not change with acid chain length, and consequently, the associated attachment energy is kept constant. The area occupied by the (100) face is almost constant and is independent of the chain length.

The second most developed form is the set of {h11} prisms. Their attachment energy increases with chain length, and consequently, their relative area decreases in the growth

Table 6. Morphology Prediction for the B_m ($P2_1/c$, $Z = 4$) and B_o ($Pbca$, $Z = 8$) Polymorphs Using the Method Based on the Attachment Energy[a]

	crystal polymorph	predicted forms	total area[b] (%)	E_{att} per molecule (kJ/mol)
$C_{16}H_{31}O_2H$	B_m[c]	{100} (2)	85.7	−7.2
		{110} (4)	5.6	−76.0
		{21$\bar{1}$} (4)	8.8	−94.1
$C_{18}H_{35}O_2H$	B_m[d]	{100} (2)	86.9	−7.2
		{110} (4)	5.2	−83.0
		{21$\bar{1}$} (4)	7.9	−104.9
$C_{18}H_{35}O_2H$	B_o[d]	{001} (2)	87.9	−7.1
		{102} (4)	5.5	−82.9
		{111} (8)	6.6	−120.1
$C_{20}H_{39}O_2H$	B_o[c]	{001} (2)	87.7	−7.1
		{102} (4)	6.3	−77.6
		{111} (8)	1.1	−127.7
		{112} (8)	4.9	−128.0

[a] The forms present in the predicted morphologies are given followed by their multiplicity (in parentheses). The attachment energy of each form and their corresponding total area are also given. [b] Total area calculated as 100 × [(total surface area of the form)/(total surface area)]. [c] Crystal structures determined from powder X-ray diffraction data. [d] Crystal structures determined from single-crystal X-ray diffraction data.[7]

Table 7. Morphology Prediction for the E_m ($P2_1/c$, $Z = 4$) and E_o ($Pbca$, $Z = 8$) Polymorphs Using the Method Based on the Attachment Energy[a]

	crystal polymorph	predicted forms	total area[b] (%)	E_{att} per molecule (kJ/mol)
$C_{18}H_{35}O_2H$	E_o[c]	{001} (2)	88.2	−7.1
		{102} (4)	5.9	−82.2
		{112} (8)	5.8	−133.9
$C_{16}H_{31}O_2H$	E_m[d]	{100} (2)	85.7	−7.2
		{110} (4)	5.8	−75.2
		{311} (4)	4.6	−94.4
		{211} (4)	3.9	−97.3
$C_{18}H_{35}O_2H$	E_m[c]	{100} (2)	86.9	−7.2
		{110} (4)	5.4	−82.2
		{11$\bar{1}$} (4)	3.5	−105.3
		{21$\bar{1}$} (4)	4.1	−108.1
$C_{20}H_{39}O_2H$	E_m[d]	{100} (2)	87.9	−7.2
		{110} (4)	5.1	−89.2
		{31$\bar{1}$} (4)	6.9	−118.9

[a] The forms present in the predicted morphologies are given followed by their multiplicity (in parentheses). The attachment energy of each form and their corresponding total area are also given. [b] Total area calculated as 100 × [(total surface area of the form)/(total surface area)]. [c] Crystal structures determined from single-crystal X-ray diffraction data.[7] [d] Crystal structures determined from powder X-ray diffraction data.

morphology, as shown in Figure 6, where E_{att}^{h11} linearly varies as a function of the carbon content of the chain. Certainly, the absolute value of the attachment energy increases with an increase in chain length because of the strengthening of lateral van der Waals interactions between parallel chains. This behavior can be rationalized in terms of the crystal packing of molecules in polymorph C. In fact, in this crystal structure, the molecules are packed forming an angle with the (h11) side face that increases when the chain length decreases (Figure 5b−d). The number of van der Waals interactions projected in the (h11) side face decreases as this angle increases, and therefore, the associated attachment energy also decreases, giving rise to more developed (h11) side faces for the shorter acids. Consequently, ticker crystals are expected for the C polymorph of shorter acids, in agreement with the experimental observations. The same variation of the parameters holds for the (h02) faces, the value of attachment energy increasing with chain length, and therefore, the associated total area decreases, accordingly (Figure 6). However, the {110} prism behaves anomalously, because the absolute value of its attachment energy increases with chain length while its morphological importance increases, too, until a maximum value of 1.4% of the total area of the crystal (Figure 6). Actually, this opposite trend is only apparent, because the {110} prism belongs to the [001] zone axis where the geometrical competition is restricted to the sole {100} dominant form.

Morphology Simulation of the Low-Temperature (A-, E-, and B-type) Polymorphs of Carboxylic Acids. Figure 7 shows the crystal morphology of the low-temperature polymorphs predicted using the attachment energy method. The experimental crystal shapes are shown in Figure 3. Predicted morphologies are quantitatively illustrated in Tables 6−8.

In summary, the calculation methodology we used is able to predict the experimental observed habits, distinguishing between needle and plate habits.

The A_{super} polymorph crystallizes from supersaturated solutions as needlelike crystals that are reproduced by the theoretical approach. There are no experimental crystals of the A_1 polymorph to compare. Predicted morphologies of the A_{super} and A_1 polymorphs are different as expected in light of their different crystal structures.

The B- and E-type polymorphs crystallize as platelike crystals with the dominant shape of a rhombus and with a very short third dimension. In these crystals, the basal faces account for 85% of the crystal surface. As a consequence of the plate-type morphologies, crystals of the C-, E-, and B-type polymorphs are expected to easily cleave in the (100) planes, as experimentally observed.

With regard to the experimental morphology, the observed platy crystals of the C-type and E- and B-type polymorphs are distinguished only by the value of the acute angle that characterizes their dominant rhombus-shaped face. In fact, the measured angle of ≅54° on the (100) face of the C form corresponds to the theoretical angle (55.65°) determined by the set of equivalent ⟨011⟩ directions while the measured angle of ≅74° on the (001) face of the B and E

Table 8. Morphology Prediction for the A_{super} ($P\bar{1}$, $Z = 6$) and A_1 ($P\bar{1}$, $Z = 2$) Polymorphs of $C_{12}H_{23}O_2H$ Using the Method Based on the Attachment Energy[a]

	crystal polymorph	predicted forms	total area[b] (%)	E_{att} per molecule (kJ/mol)
$C_{12}H_{23}O_2H$	A_{super}[c]	{011} (2)	46.7	−20.2
		{01$\bar{1}$} (2)	41.9	−22.4
		{1$\bar{3}\bar{3}$} (2)	9.6	−84.3
		{1$\bar{1}\bar{3}$} (2)	1.8	−86.0
$C_{12}H_{23}O_2H$	A_1[c]	{001} (2)	37.1	−44.6
		{10$\bar{1}$} (2)	26.9	−47.9
		{100} (2)	5.7	−55.4
		{01$\bar{1}$} (2)	20.4	−63.8
		{11$\bar{2}$} (2)	9.8	−66.2
		{1$\bar{1}$1} (2)	0.1	−77.5

[a] The forms present in the predicted morphologies are given followed by their multiplicity (in parentheses). The attachment energy of each form and their corresponding total area are also given. [b] Total area calculated as 100 × [(total surface area of the form)/(total surface area)]. [c] Crystal structures determined from single-crystal X-ray diffraction data.[7]

forms corresponds to the theoretical angle (74.21°) determined by the set of equivalent ⟨110⟩ directions.

Then, the just mentioned angles are strictly related to the ratio of the two-dimensional cell parameters of the dominant {*hkl*} form of these layered compounds, as it already followed from morphological measurements conducted on single, twinned, and polytypic crystals of *n*-alcohols[24] and long chain *n*-paraffins.[10]

Conclusions

Prediction of the morphologies of the high- and low-temperature polymorphs of carboxylic acids using methodologies with an increasing degree of sophistication has shown that the method based on the calculated attachment energy for each growing face gives the most accurate representation of the observed solution-grown crystal shapes. The BFDH laws give valuable information to limit the number of possible growing faces to be studied by energy-based approaches. Other authors such as S. L. Price[25] and D. S. Coombes[18] also observed these general tendencies when modeling the crystal morphology of pharmaceuticals.

The feasibility of a given carboxylic acid polymorph crystallizing yielding platelike or acicular crystals can be rationalized in terms of the arrangement of the terminal methyl and carboxyl groups within the crystal lattice (Scheme 1). Molecules in the C-, E-, and B-type polymorphs consist of alternated bilayers of carboxylic acid dimers giving rise to terminal planes of only weak van der Waals methyl−methyl interactions compared to stronger hydrogen bond interactions inside the bilayer. Therefore, the probability of a new layer to attach to this weakly interactive (100) face is small. The (100) face has the slowest growth rate, and therefore, it is the most developed. Molecules in the A_{super} polymorph have carboxyl and methyl terminal groups coexisting in the same layer which enhances the attachment of crystallization units in a direction that maximizes the number of strong interactions, hydrogen bonds in this system. The growth in one direction produces elongated crystals.

Assuming a layer-by-layer growth mechanism, the morphology of the different polymorphs can be rationalized in terms of the attachment energy associated with each growing face, and therefore, the acicular and plate morphologies can be fully understood.

It is clear that the solvent used for crystallization of many organic solutes strongly influences the final crystal morphology. Nevertheless, the effect of solvent on the habits of the carboxylic acid polymorphs grown from solution has never been observed experimentally. Thin plates are obtained for the C-, E-, and B-type polymorphs and acicular habits for the A-type polymorph in a manner independent of the crystallization solvent.

In this case, the predicted morphologies have shown that there should be no large differences in the solvent−solute intermolecular interactions at the various crystal faces because all faces are formed by hydrophobic C−H sites. Thus, for the different polymorphs of carboxylic acids, the crystal morphology is well-reproduced in a manner independent of the solvent considered. This is not the case, for example, with dicarboxylic acids such as succinic acid[11,23] in which hydrophobic and hydrophilic faces are identified and the habit is controlled by the solvent polarity, plate crystals are obtained from polar solvents like water and ethanol, and fragile needles are obtained from nonpolar solvents like benzene and toluene.

Acknowledgment. We thank the Ministerio de Ciencia y Tecnología (MAT2008-00497), Consolider-Ingenio 2010 through La Factoria de Cristalización (CSD2006-15), Generalitat de Catalunya through Xarmae (Xarxa de referència d'R+D+I en Materials Avançats per a l'Energia), and the Grup Consolidat de Cristal·lografia (SGR 2009 1307) for financial support.

Supporting Information Available: Description of the force field selection. This material is available free of charge via the Internet at http://pubs.acs.org. CCDC entries 785083 ($C_{16}H_{31}O_2H$, B_m polymorph), 785084 ($C_{16}H_{31}O_2H$, E_m polymorph), 785081 ($C_{20}H_{39}O_2H$, B_o polymorph), and 785082 ($C_{20}H_{39}O_2H$, E_m polymorph) contain the supplementary crystallographic data for this paper. These data can be obtained free of charge from The Cambridge Crystallographic Data Centre via www.ccdc.cam.ac.uk/data_request/cif.

References

(1) Tedesco, E.; Giron, D.; Pfeffer, S. *CrystEngComm* **2002**, *4*, 393.
(2) Beyer, T.; Day, G. M.; Price, S. L. *J. Am. Chem. Soc.* **2001**, *123*, 5086.
(3) (a) Pagola.; et al. *Nature* **2000**, *404*, 307. (b) Buller, R.; Peterson, M. L.; Almarsson, O.; et al. *Cryst. Growth Des.* **2002**, *2*, 553.
(4) (a) Aguiló, M.; Woensdregt, C. F. *J. Cryst. Growth* **1984**, *69*, 527. (b) Solans, X.; Font-Altaba, M.; Aguiló, M.; et al. *J. Appl. Crystallogr.* **1983**, *16*, 637.
(5) Rohl, A. L. *Curr. Opin. Solid State Mater. Sci.* **2003**, *7*, 21.
(6) (a) Moreno, E.; Cordobilla, R.; Calvet, T.; et al. *New J. Chem.* **2007**, *31*, 947. (b) von Sydow, E. *Ark. Kemi* **1956**, *9*, 231. (c) Sato, K.; Kobayashi, M. *Crystals 13*; Springer-Verlag: Berlin, 1991. (d) Goto, M. *J. Jpn. Oil Chem. Soc.* **1987**, *36*, 909. (e) Gbabode, G.; Négrier, P.; Mondieig, D.; et al. *Chem.—Eur. J.* **2007**, *13*, 3150.
(7) For the crystalline structure coordinates, see the following. E_m form: (a) Kaneko, F.; Kobayashi, M.; Kitagawa, Y.; Matsuura, Y. *Acta Crystallogr.* **1990**, *C46*, 1490–1492. C form: (b) Bond, A. D. *New J. Chem.* **2004**, *28* (1), 104. Moreno, E.; Cordobilla, R.;

Calvet, T.; et al. *Acta Crystallogr*. **2006**, *C62*, 131. E_o form: (c) Kaneko, F.; Sakashita, H.; Kobayshi, M. *Acta Crystallogr*. **1994**, *C50*, 247. B_m form: (d) Goto, M.; Asada, E. *Bull. Chem. Soc. Jpn*. **1978**, *51* (9), 2456. B_o form: (e) Kaneko, F.; Sakashita, H.; Kobayshi, M. *Acta Crystallogr*. **1994**, *C50*, 245. A_{super} form: (f) Goto, M.; Asada, E. *Bull. Chem. Soc. Jpn*. **1978**, *51* (1), 70. A_1 form: (g) Lomer, T. R. *Acta Crystallogr*. **1963**, *16*, 984.

(8) Moreno, E.; Cordobilla, R.; Calvet, T.; et al. *Chem.—Eur. J*. **2009**, *15*, 13141.

(9) Moreno, E. *On the Polymorphism and structural characterization in the family of even saturated carboxylic acid*, European Ph.D. Thesis, **2008**, Universidad de Barcelona c/Martí I Franquès sn CP.08028, Barcelona, Spain.

(10) (a) Aquilano, D. *J. Cryst. Growth* **1977**, *37*, 215. (b) Boistelle, R.; Aquilano, D *Acta Crystallogr*. **1977**, *A33*, 642. (c) Boistelle, R.; Aquilano, D. *Acta Crystallogr*. **1978**, *A33*, 406. (d) van Hoof, P. J. C. M.; Grimbergen, R. F. P.; Meekes, H.; et al. *J. Cryst. Growth* **1998**, *191*, 861. (e) Bennema, P.; Liu, X. Y.; Lewtas, K.; et al. *J. Cryst. Growth* **1992**, *121*, 679. (f) Liu, X. Y.; Bennema, P. *J. Cryst. Growth* **1994**, *135*, 209. (g) Rubbo, M.; Boistelle, R. *J. Cryst. Growth* **1981**, *51* (3), 480. (h) Madsen, H. E. L.; Boistelle, R. *J. Cryst. Growth* **1979**, *46* (5), 681.

(11) (a) Davey, R. J.; Mullin, J. W.; Whiting, M. J. L. *J. Cryst. Growth* **1982**, *58*, 304. (b) Van der Voort, E. *J. Cryst. Growth* **1991**, *110*, 662. (c) Pfefer, G.; Boistelle, R. *J. Cryst. Growth* **2000**, *208*, 615. (d) Docherty, R.; Roberts, K. J. *J. Cryst. Growth* **1988**, *88*, 159.

(12) Hollander, F.; Boerrigter, S. X. M.; van de Streek, J.; Bennema, P.; Meekes, H.; Yano, J.; Sato, K. *J. Phys. Chem. B* **2003**, *107*, 5680.

(13) Bravais, A. *Etudes Crystallographiques*; Academie des Sciences: Paris, 1913.

(14) Friedel, G. *Bull. Soc. Fr. Mineral*. **1907**, *30*, 326.

(15) Donnay, J. D. H.; Harker, D. *Am. Mineral*. **1937**, *22*, 463.

(16) Hartman, P.; Perdok, W. G. *Acta Crystallogr*. **1955**, *8*, 49.

(17) (a) Hartman, P.; Bennema, P. *J. Cryst. Growth* **1980**, *49*, 145. (b) Hartmaan, P. *J. Cryst. Growth* **1980**, *49*, 157.

(18) Coombes, D. S.; Catlow, R. A.; et al. *J. Pharm. Sci.* **2002**, *91*, 1652.

(19) Docherty, R.; Clydesdale, G.; Roberts, K. J.; et al. *J. Phys. D: Appl. Phys*. **1991**, *24*, 89.

(20) *Materials Studio Modeling*, version 4.2. http://accelrys.com/products/materials-studio.

(21) Sun, H. *J. Phys. Chem. B* **1998**, *102*, 7338.

(22) Bernstein, J.; Davis, R. E.; Shimoi, H. L.; Chang, N. L. *Angew. Chem., Int. Ed*. **1995**, *34*, 1555.

(23) Berkovitch-Yellin, Z. *J. Am. Chem. Soc*. **1985**, *107*, 8239.

(24) Amelinckx, S. *Acta Crystallogr*. **1956**, *9*, 217.

(25) Brunsteiner, M.; Price, S. L. *Cryst. Growth Des*. **2001**, *1*, 447.